Geomechanics and Engineering, *Vol. 25, No. 5 (2021) 357-371*
DOI: https://doi.org/10.12989/gae.2021.25.5.357

Model studies on polymer strip reinforced soil retaining walls

Mehmet R. Kahyaoğlu*[1] and Mehmet Şahin[2a]

[1]*Department of Civil Engineering, Faculty of Engineering, Muğla Sıtkı Koçman University, Muğla, Turkey*
[2]*Ministry of Youth and Sports– General Directorate of Investment and Enterprises, Ankara, Turkey*

(Received September 7, 2020, Revised April 21, 2021, Accepted May 19, 2021)

Abstract. Polymer strip (PS) reinforced soil retaining walls (RSRW) are in common use due to the associated construction speed, ease of use, aesthetic appeal and low cost. It is quite significant to estimate the deformation behavior of this types of walls before construction. In this study, firstly, a full-scale field model of PS-RSRW was constructed and instrumented. According to the experimental result, the maximum measured displacements occurred at 30% of the height down from the top of the wall. The maximum tensile loads in the reinforcements were measured at a distance of 40% of the wall height from the face of the wall. Then, a two-dimensional (2D) finite element method (FEM) model was established and calibrated with experimental data from the field model. The predicted displacements of the wall facing showed reasonable agreement with the measured deformations. The reinforcement loads calculated from the validated FEM model were also compared with theoretical methods. Finally, RSRW having different heights were numerically modeled with various combinations of materials utilized for filling and reinforcement. The effects of parameters such as wall height (H), reinforcement length (L) and reinforcement interval (Sv) on the horizontal wall displacement and on the reinforcement loads are investigated through parametric analyses.

Keywords: geosynthetics; reinforced soil; retaining wall; instrumentation and monitoring; numerical analyses; earth pressure

1. Introduction

Reinforced soil retaining walls (RSRW) were first developed and promoted by French engineer Henri Vidal in 1960s. RSRW have been used intensively since the beginning of 1970s due to their resistance to corrosion and other reactions, their flexibility, their easier and faster construction, and lack of any need for large foundation structures or concrete wall sections (Vidal 1969, Lee *et al.* 1973, Whitcomb and Bell 1979).

RSRW are generally formed out of three structural units: reinforcement to improve the tensile strength properties of the bulk soil, fill material and facing elements to retain the soil between the reinforcement layers (Holtz *et al.* 1997, Holtz and Lee 2002). Horizontal reinforcements inside the soil are utilized to reduce the lateral displacements that occur as a result of axial loading on the granular fill material (Kaya 2007). After 1980s, in particular, reinforcement came to vary in design from inextensible steel reinforcing strips to geotextiles, geogrids and polymeric strips (Güler 2006, Mahmood 2009, Liu *et al.* 2017). Facing elements, which retain the fill material and provide an aesthetic appearance, make no contribution to the stability of the structure and can be composed of prefabricated modular blocks, concrete panels, shotcrete, metal plates, or timber. A connection between the facing elements and continuous reinforcement can be achieved with non-point friction (Seed and Whitman 1970). The fill to be used in the reinforced area should be of high quality, and should meet the specifications for the construction of roadway embankments, featuring low compressibility, durability and drainage properties (Segrestin and Bastick 1988). It is known that thousands of RSRW have been constructed over the past 30 years (Elias *et al.* 2001). All above referenced studies have had an impact on the design of RSRW.

RSRW technologies largely depend on the stress transfer between the sliding soils to the reinforcement through friction at the non-yielding soil-reinforcement interface (Christopher *et al.* 1990, Jones 1996, Sawicki 2000, Balaban and Onur 2018). Hence, the lateral thrust against the facing elements are resisted with the help of reinforcement tensile strength. The design of a RSRW depends on the determination of the dimensions and requirements of the reinforcements taking into account both the external and internal failure mechanisms known as the limit state (Segrestin and Bastick 1988, Leshchinsky and Han 2004). Wall design is based on an examination of the sliding mass and wall deflection around the wedge (external stability) rupture, pulling outwards, and the elongation of reinforcement (internal stability) (Altunbas *et al* 2017, Kayadelen *et al.* 2018). In terms of stability, the reinforcement type and strength parameters of the fill material and the reinforcement are the most significant criteria (Yang *et al.* 2013).

In recent years, model experiments have been carried out to determine deformations, to examine the interface behavior between soil and reinforcement, to interpret the

∗Corresponding author, Assistant Professor
E-mail: rkahyaoglu@mu.edu.tr
[a]Ph.D. Student
E-mail: mehmetsahin1986@gmail.com

ISSN: 2005-307X (Print), 2092-6219 (Online)

facing effect and to improve existing design methods (Bathurst *et al.* 2008, Castorina *et al.* 2015, Allen and Bathurst 2014, Allen and Bathurst 2015, Allen and Bathurst 2018). Reinforcement loads could be predicted with the K-Stiffness Method using large database of measured strains (Bathurst *et al.* 2008) under working stress conditions. This method has large emprical components including reinforcement stiffness and facing stiffness and assumes a triangular distribution of loads at constant vertical reinforcement spacing. Allen and Bathurst (2015) investigated the influence of parameters such as reinforcement stiffness, facing stiffness, soil stiffness, reinforcement spacing and facing batter on maximum reinforcement load and proposed Simplified Stiffness Method. The active earth pressure coefficient is used as an index value and can be applied on the cohesive-frictional backfill soils. Computation of maximum reinforcement loads at the end of construction and over the design life are the additional considerations.

Bourgeois *et al.* (2011) and Ehrlich and Mirmoradi (2013) investigated the behavior of RSRW under static loads by conducting full-scale experiments. The aim of the studies was to understand the deformation behavior of RSRW, both throughout the construction process and under surcharge loadings, creating a large database of experimental results from instrumented walls and developing design methodologies for RSRW. Bathurst *et al.* (2000) constructed experimental setups to compare the use of different facing elements, aiming to determine the performance of RSRW, aiming use of high-quality data for the calibration of numerical models. The authors observed that strain was lower in walls with more rigid facing elements, while the highest loading values were identified at the connection points of the wall. Hatami and Bathurst (2005) constructed a more comprehensive database as part of their effort to develop current and future design tools and built experimental setups through which they investigated the impact of changes in fill and reinforcement materials.

The limit loads, wall displacements and reinforcement tension stresses were compared for each test. Abdelouhab *et al.* (2011) carried out an experimental study to compare geosynthetic reinforcement with metal reinforcements, and stated that geosynthetic reinforcements offered twice the benefit of their metal counterparts regarding wall stability and adherence. The internal behavior of reinforced soil masses is dependent on such parameters as soil friction, cohesion, interface shear stiffness and reinforcement strength, all of which are significant in wall design. The authors also indicated that strength parameters of soil have a higher impact on wall deformation than the reinforcement strength parameters.

Numerical modeling methods were developed to expand the limited database of physical data. The FEM model is one of the most commonly used numerical modeling approaches in the design and analysis of RSRW. FEM model are validated through the calibration of computed results with measured results of real reinforced retaining wall. The researchers mentioned the significance of soil strength parameters and they highlighted that the use of high-quality materials, proper field inspections and accurate wall measurements to increase the accuracy of numerical modelling (Abdelouhab *et al.* 2011, Allen and Bathurst 2002, Bathurst *et al.* 2009, Cristelo *et al.* 2016, Hatami and Bathurst 2005, Horpibulsuk *et al.* 2011, Kongkitkul *et al.* 2010, Mendonça *et al.* 2003, Riccio *et al.* 2014, Salem *et al.* 2018, Vieira *et al.* 2011, Yang *et al.* 2012, Yang *et al.* 2014, Yu *et al.* 2015 and Yu *et al.* 2016, Song and Tian 2019).

Huang *et al.* (2009) constructed a full-scale RSRW and performed finite element analyses to understand the effects of loading conditions, reinforcement and soil properties, and material models. In their study, three different soil models were developed with welded wire mesh geogrid reinforcements and the computed results were compared with the front-face displacements, the loads on connections and reinforcement strains. Bourgeois *et al.* (2011) generated a FEM model to assess deformation, displacement and stress variations under larger loads, and illustrated the importance of parameter prediction of the soil and reinforcement in determining the deformation behavior of RSRW. Ouria *et al.* (2016) investigated the performance of retaining wall reinforced with carbon fiber reinforced polymer using numerical model. The FEM used to understand the deformation behaviour of RSRW was verified with the experimental results of a reference wall.

In all the above mentioned studies, in general, the wall height (H) varied between 2 to 4 m, the reinforcement length (L) was between 0.6 and $0.8 \times H$, and the reinforcement interval (Sv) was between 0.4 and 1 m. The slope of the front face was usually made an angle of 8° to the vertical axis. The fill material, in general, had a unit weight ranging from 16 to 20 kN/m^3 and an internal friction angle varying between 30 to 38°. Reinforcement materials with a tensile strength of 10 to 200 kN/m were chosen (Bathurst *et al.* 2008, Allen and Bathurst 2014, Allen and Bathurst 2015, Ouria *et al.* 2016). Displacement gauges and strain gauges were utilized to measure the wall displacements and the strain in the reinforcement, respectively. In order to ascertain the loads acting on the reinforcements, extensometers and potentiometers were used to identify the strain of the reinforced region. Furthermore, settlement plates were applied for fill subsidence. Due to the wall movement resulting from surcharge load, vertical displacement diminished getting further away from the wall. Still dependent on the applied surcharge, the maximum movement of the wall outwards was 2-4% of its height (H). The measured horizontal soil stresses were lower than the theoretical earth pressures and closer to the FEM model analysis results. From the FEM model analyses, the maximum horizontal displacements formed on the front face of the wall at the H/3 level were ranged from 0.9 to 2.5% of its height (Christopher *et al.* 1990, Fattah *et al.* 2009). It was determined that strains on the wall surface increased with wall depth, such that the maximum unit deformations were formed on the wall front and the strain effects generally increased with the depth up to a certain limit (Collin 1997). When reinforcement strength was increased, smaller displacements were observed, and so it was recommended to use reinforcements with a higher resistance.

2. Scope and objective

The study aims to understand the deformation behavior of PS RSRW under working stress conditions. A 3m high

polymer strip reinforced retaining wall was constructed and instrumented with pressure cells, potentiometers, and strain gauges. After the wall construction process, the vertical load was applied to the upper surface of the fill material and was increased up to a final load of 20 kPa. The location and magnitude of the maximum loads acting reinforcements were investigated. Measured loads on reinforcements were checked using theoretical methods. The location and magnitude of the horizontal displacement of facing elements were also determined.

Two-dimensional numerical simulation of the field model was created and the verification of the FEM Model was carried out. After the necessary confirmations, the effects of wall height (H), reinforcement length (L) and the strength properties of the reinforcement and fill materials on the maximum horizontal displacements and the tensile stresses, were determined through parametric analyses. As a result of parametric analysis, the effects of parameters such as reinforcement stiffness, reinforcement length, filling stiffness, wall height on the deformation behavior of the reinforced wall are determined. We have made suggestions that we think it will benefit the designers a lot about the location and size of the maximum deformation and the location and size of the load acting on the reinforcement.

3. Field model

3.1 Material properties

Drawing upon the guides (Collin 1997, AASHTO 2002, Elias and Christopher 1996), mixtures of sand, gravel and silt were formed granulometrically as the fill material (F) and its index properties and shear strength parameters were determined (see Table 1).

The fill material was a silty-sand with gravel, some parameters were experimentally measured as elastic modulus (E=32 MPa), Poisson's ratio (ν=0.3) and internal friction angle (ϕ'=36°). The fill material was heavily compacted to a relative density of 94%. After compaction, it was aimed to achieve a bulk unit weight of 21.0 kN/m^3, based on the maximum dry unit weight and optimum water content values of 19.0 kN/m^3 and 10%, respectively, obtained from a standard Proctor test. The interface peak and residual shear strength properties of the unreinforced and reinforced filler material were determined in direct shear test. For the reinforced fill case, as well as the current conventional testing method for direct shear test, the reinforcement is placed at the boundary between the lower and upper boxes.

The wall was reinforced with polymer strips (PS) as a relatively low resistant and extensible reinforcement material that permit significant wall deformations, especially under surcharge loads. PS were produced mainly from polyethylene and polyamide coated polyester fiber. Furthermore, PS supplied from local producers were used for wall reinforcement. The properties of PS reinforcements determined in the laboratory are presented in Table 2. The length of the polymer strip reinforcements was selected as 70% of the wall height (Bilgin and Mansour 2014). The reinforcement layers were laid horizontally and vertically at 30 cm and 60 cm intervals, respectively.

Table 1 Index properties of fill material

Filler material		Filler F	Drainage D
Gravel content (%)		15	100
Sand content (%)		70	-
Silt content (%)		15	-
Uniformity coefficient; C_u		70.67	16.32
Coefficient of curvature; C_c		1.23	1.09
Unit weight; γ (kN/m^3)		21	22
Maximum dry unit weight; $\gamma_{dry,max}$ (kN/m^3)		19	20
Optimum water content; w_{opt} (%)		10	-
Internal friction angle (°)	$\phi'_{residual}$	36	38
	ϕ'_{peak}	38	40

Table 2 Properties of polymer strip

Reinforcement material	Polymer strip PS
Tensile strength (kN/m)	11.2
Strain (%)	13.4
Tensile strength @2% strain (kN)	2.1
Tensile strength @5% strain (kN)	3.4
Thickness (mm)	3.12
Internal friction angle of interface between filler and reinforcement (°)	24

Prefabricated modular blocks (60 cm in width, 60 cm in height, and 10 cm thick) were used as facing elements. A non-reinforced concrete foundation, 50 cm deep and 150 cm wide, was built to guide the installation of the concrete blocks.

3.2 Design of field model and experimental procedure

A PS RSRW measuring 3.0 m in height, 5.0 m in depth and 2.4 m in width was bordered on three sides (the back and two sides) by compacted fill acting as if it were a real rigid system. This arrangement was selected to ensure that deformations were generated only on the facing elements.

The plan and the section views of the field model are presented in Fig. 1. In the plan, a one-meter wide section in the center was chosen as the instrumentation region (50 cm wide areas at the margins were not instrumented) and for each field test, 32 measurement devices were used in total.

A total of 24 strain gauges were placed on the PS reinforcements to measure unit elongation; three potentiometers were placed on the surface of facing elements to measure the horizontal wall displacement; one pressure cell was placed in the fill material to measure vertical earth pressure, and four pressure cell were placed on the facing elements to measure the horizontal earth pressure. A 32-channel data logger was used to digitize the data provided by the measurement instruments throughout the experimental study, and the obtained data was converted to the desired measurement units.

All horizontal movements and unit strain changes in the reinforced zone were measured with Tokyo Sokki Kenkyujo

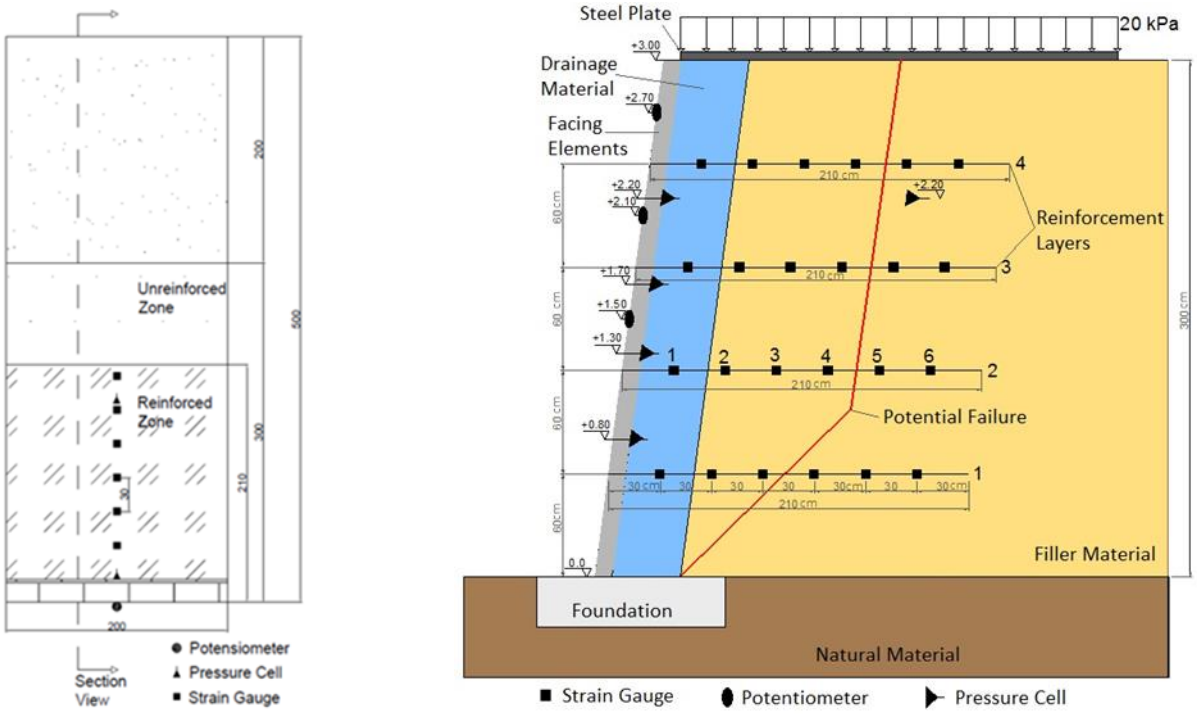

(a) Plan view (b) Section view

Fig. 1 Schematic diagram of the test walls with instrumentation

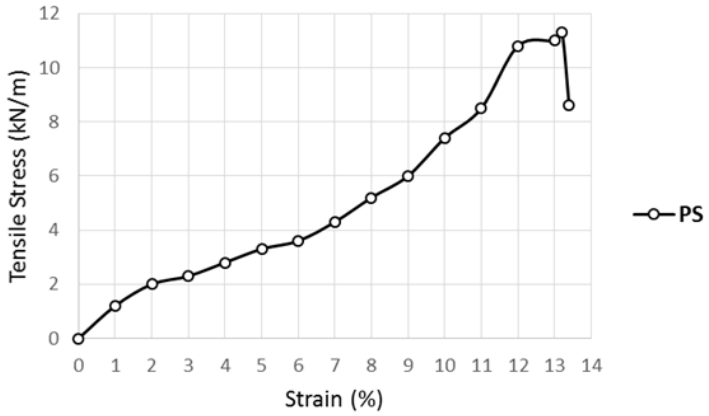

Fig. 2 Strain gauge calibration

model PL-60-11-5L strain gauges, determining the loads acting on the reinforcements. In the field model, 24 strain gauges in total were placed, six for each of the four reinforcement layers. The first strain gauge was placed at a distance of 300 mm from the front face of the retaining wall. A distance of 300 mm was left between two strain gauges. The properties of strain gauges were 60 mm in length, 120 ohms resistance, and 0.8% transverse sensitivity with a capacity of $\pm 5000 \times 10^{-6}$ strain. In order to prevent strain gages placed on the reinforcement from being damaged by the fill material during the test, polyethylene tubes were used. The strain measurements of the strain gages in polyethylene tubes were taken by means of small-diameter cables passed through the fill material.

All strain gauges were elongated to obtain deformations associated with the outward movement of the wall and the cables were extended parallel to the front face in case of the development of potential sliding planes from the reinforced soil area.

In the field model, horizontal displacement measurements were identified using the data from potentiometers fixed vertically to a steel frame mounted on the front-facing elements. To determine the horizontal displacement of the front facing elements, potentiometers were placed at 150 cm, 210 cm and 270 cm from the bottom of the wall, where they would be exposed to the greatest horizontal displacements. For this purpose, potentiometer with linear resistance–position transformers capable of measuring up to 100 mm were used. The total station device was also used in the topographic measurements, comprising six vertical steel survey bars mounted on the wall face. Measurements were taken at 10 survey points placed at 300 mm-intervals on the front face of the wall after each fill construction and each surcharge increase.

(a) Placing polymer strip reinforcements

(b) Close view of drainage layer

(c) General overview of wall and prefabricated front face elements

Fig. 3 Pictures taken from different stages of construction of the wall

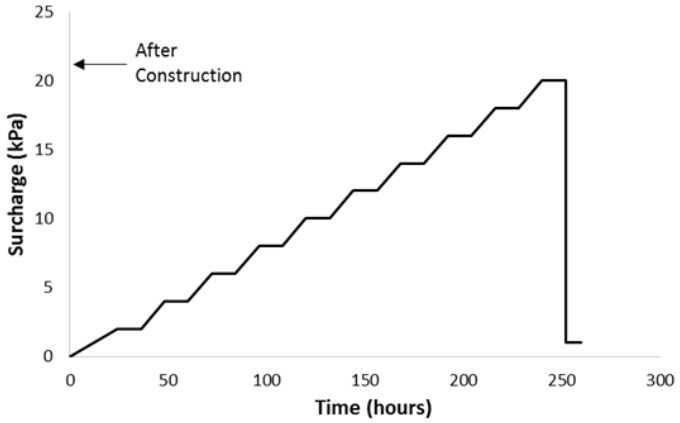

Fig. 4 Construction sequence

In the site model, five Tokyo Sokki Kenkyujo model KDE-200KPA pressure cells were used; one placed at the level of 220 cm above the wall base between the front facing elements and the filler material to measure vertical soil pressure, and the other four set on the facing elements at the levels above the wall base of 80 cm, 130 cm, 170 cm and 220 cm to measure horizontal soil pressure. Considering that the front face inclination, rubber pads were placed between the pressure cells and the face elements. In this way, both the pressure cells could be placed vertically and they were prevented from being crushed between the facing element and the moving soil.

One of the horizontal pressure gauges was positioned at the same level as the vertical pressure gauge to determine the ratio of lateral soil pressure to vertical soil pressure (K). The pressure gauge had a capacity of 200 kPa and a strain measurement limit of 672×10^{-6}. The calibration coefficient was 0.298 kPa/1×10^{-6}.

3.3 Calibration

It was necessary to calibrate the potantiometers, strain gauges and pressure cells to be used during the field tests. The calibration test of the strain gauges involved tensile tests of the polymer strip samples measured with a strain gauge utilizing a universal testing machine (UTM) by applying constant rate of extension (%10strain/min≈30 mm/min)(the width of the tested strip is 9cm, while the length is 30 cm). The strain gauges were placed in the middle lane of the PS specimens, and strain measurements were taken at each strain rate. The load-strain curve for PS at constant strain rates is shown in Fig. 2. The voltage values obtained from the strain gauge were associated with the elongation and the tensile stress on the polymer strip.

3.4 Test wall construction and loading

The wall back side was covered with a 30 cm of fill material and compressed with a hand-plate compactor, with prefabricated front face elements placed in front. PS reinforcements were placed on two compacted fill layers (the distance between reinforcement layers, S_v was 60 cm).

The compaction process was carried out in two different ways: heavy and light compaction. In order to minimize the

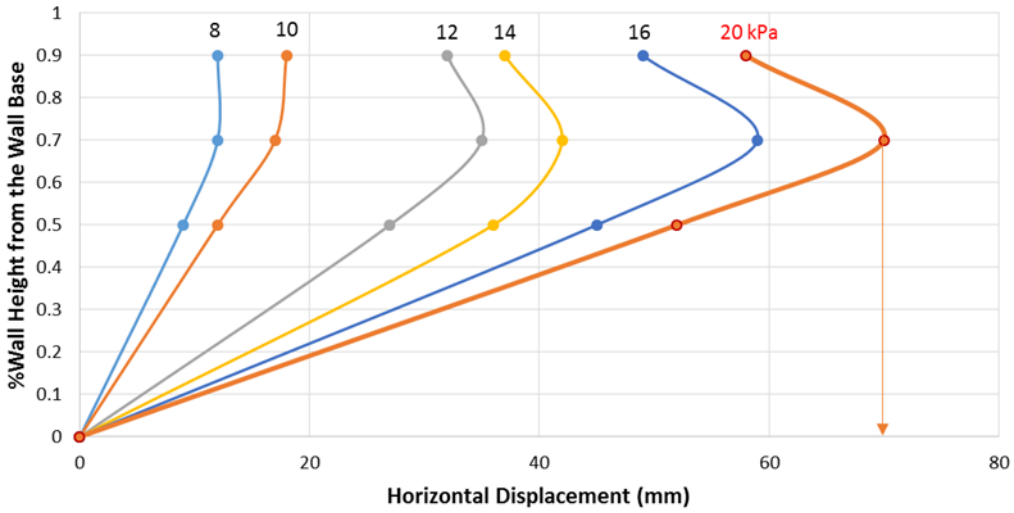

Fig. 5 Horizontal displacement of wall face

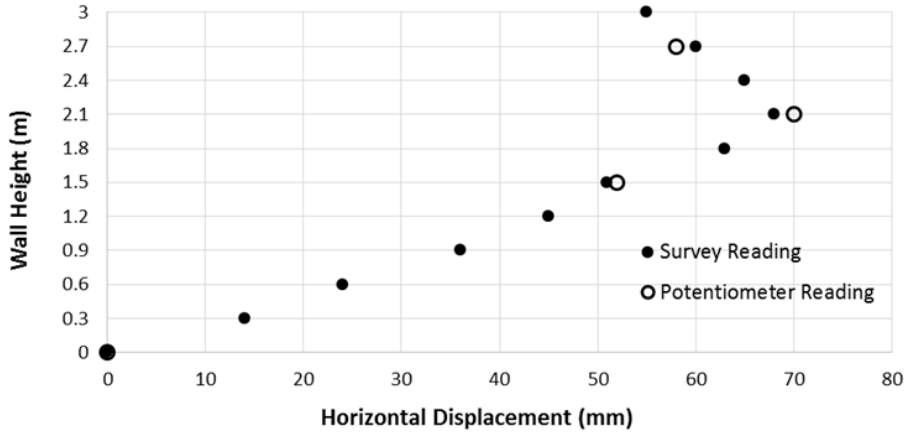

Fig. 6 The measured horizontal displacement of the wall face identified from the survey and the potentiometers

deformation caused by horizontal earth pressure, 40 cm from wall surface distance where the drainage material is placed, only light compaction was applied. For the other parts of the fill, heavy compaction was applied. Using a hand compactor for each layer, the light compaction lasted 10 minutes and the heavy compaction lasted 30 minutes. The wall construction process is demonstrated in Fig. 3.

A plate with a dimension of 1000 mm × 3000 mm × 5 mm was placed on the upper surface of the instrumented filler material, and the surcharge load was applied to the wall by means of a plastic tank (1000 mm wide × 3000 mm long × 2000 mm deep) positioned on this steel plate (considering the applied load, the load of steel plate is neglected). The load was increased through the filling of the tank with water at a constant flow rate, up to a final load of 20 kPa applied in 2 kPa increments every 24 hours. The total construction time of the wall was 250 hours. Fig. 4 shows the development stages of the surcharge load.

4. Evaluation of the experimental data

4.1 Comparison of horizontal displacements

The horizontal displacements were measured at 1.5 m, 2.1 m and 2.7 m from the wall base. Fig. 5 shows the change in horizontal displacement that occurred in the wall accordingly the increase in the surcharge load. The site of the maximum horizontal displacement was observed at a point up approximately 70% of the wall height from the base. The maximum displacement of the wall at 20 kPa surcharge loading was approximately 69 mm corresponding to 2.3% of the wall height.

The general trend in the variation of wall horizontal displacements from the survey measurements and the variation of the potentiometer measurements at points along the height of the wall showed reasonable agreement (see Fig. 6). The measured horizontal displacements identified from the survey and the potentiometers were greater than the strip elongations values, the latter does not consider the global movements of the fill material.

4.2 Comparison of reinforcement strains

As a result of the tensile tests performed in the laboratory, the stress strain values were determined by means of the strain gage on the reinforcement. A calibration coefficient is needed to convert these values to the true global strain values determined as a result of the field test. Thanks to this calibration coefficient, the true global strains

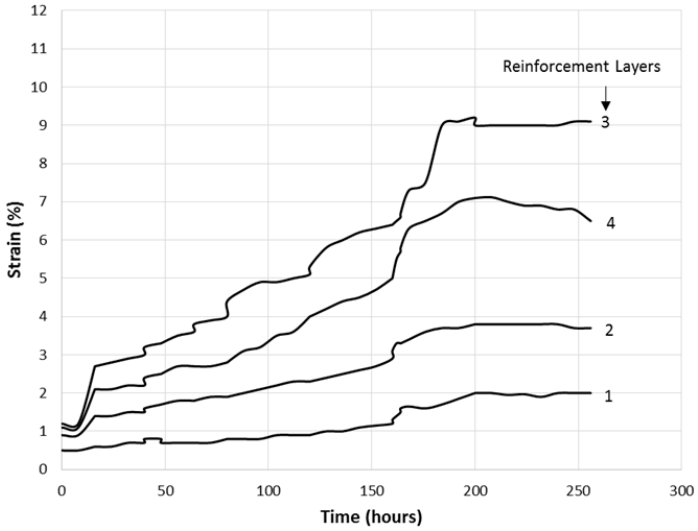

Fig. 7 Elongation on reinforcement layers

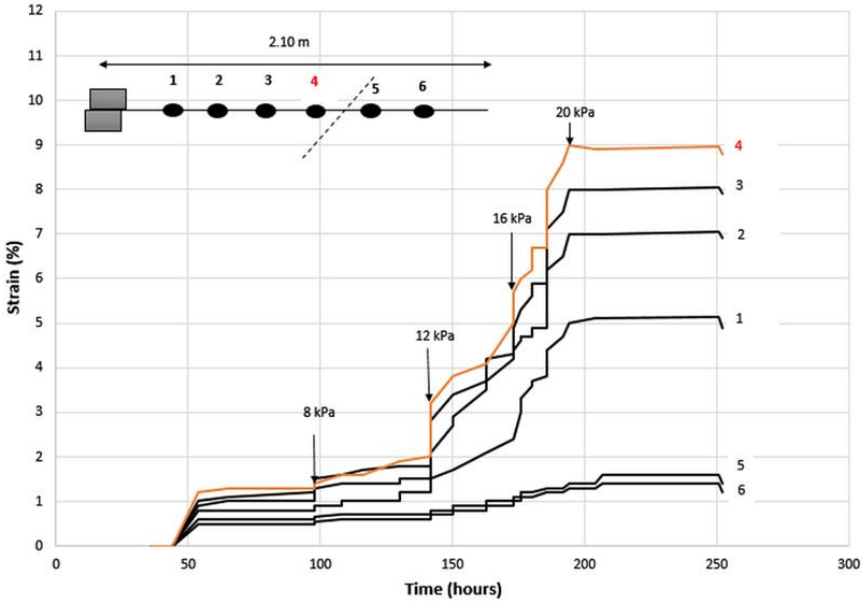

Fig. 8 Elongations on the third layer of reinforcement

via tensile tests in laboratory should be converted field strain gauge readings (local strains). (Fig. 2) (Perkins and Lapeyre 1997; Bathurst *et al.* 2002). Calibration factor (CF) of 2.24 was concluded for PS. This value is quite similar with the reported literature. Strain gauge CFs from laboratory tests on different geosynthetic products are given as 1.25 up to a local strain of 4%, and which are 2.2 for higher strains (Allen and Bathurst 2002).

Fig. 7 shows the variation of corrected reinforcement elongations recorded under the surcharge load. Each jump in the curves corresponds to a new surcharge load application. This still increased up until the next load was applied, but was followed by a decreasing rate time-dependent deformation. As expected, after the removal of the surcharge loading, it was observed that displacements in each reinforcement layer were largely irrecoverable. It was determined that the horizontal displacement value at the third reinforcement layer was 4 to 5 times greater than that observed for the lowest reinforcement level.

The 9% corrected strain value measured in the reinforcement layers is considerably higher than the elongation observed in the geosynthetic materials utilized in RSRW. Won and Kim (2006) summarized that the maximum deformation values as 2.3% in geogrids, 2.9% in woven geotextiles and 9% in nonwoven geotextiles, which corresponds to that of this study. With this elongation advantage provided by the PS material, the reinforcements can carry more loads.

In Fig. 8, the elongations recorded from the strain gauges located on the third layer of polymer strip reinforcement are shown. The time-dependent deformation of the reinforcement layer was explicitly present in the data. The most prolonged strain gage between the sliding surface and the wall is seen as number 4, and the level of elongation decreases when getting closer to the wall face. The lower strain recorded close to the wall may be assignable to the

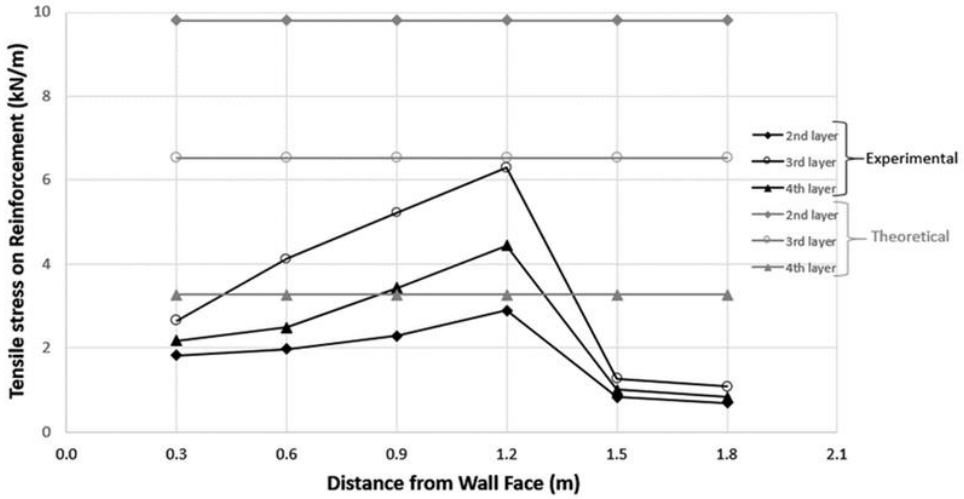

Fig. 9 Measured tensile stresses on reinforcement layers after 20kPa surcharge load application

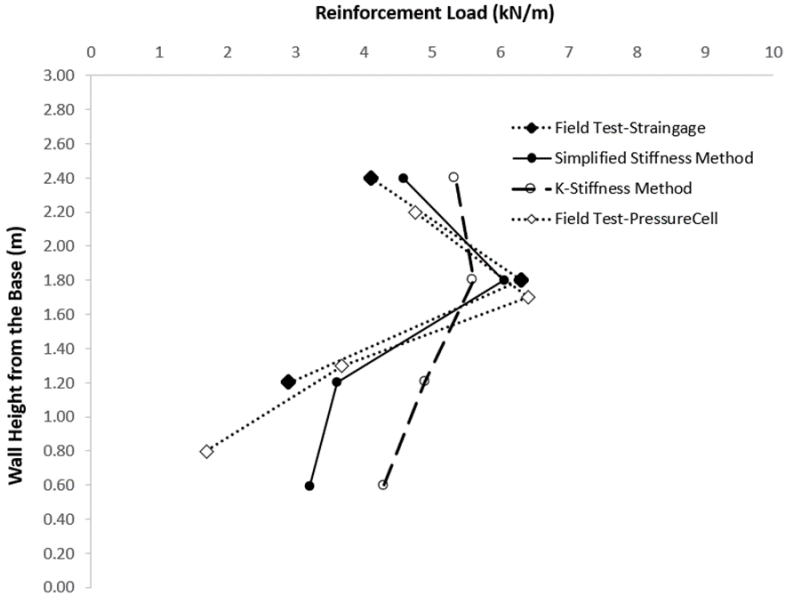

Fig. 10 Variation of reinforcement load distribution with depth based on field measurements and other design approaches

mechanism of low load transfer between points with relatively low deformation difference. The grains are overlapping each other and forming arching towards the wall surface. The elongation in the non-slip area was around one-sixth of the maximum elongation.

4.3 Comparison of tension stresses

The K-stiffness method Bathurst *et al.* (2008) was applied to predict the maximum load acting on reinforcements of RSRW. There are some complexities for the determination of the stiffness parameters of both the fill material and the facing. In order to overcome the shortcomings of this method, Allen and Bathurst (2015) and Allen and Bathurst (2018) developed a Simplified Stiffness method. In the proposed formula, the maximum reinforcement load is dependent on wall height, unit weight of fill material, active lateral earth pressure coefficient, reinforcement vertical spacing, load distribution factor and influence factors including cohesion of fill material, stiffness of both reinforcement and facing, and face batter. Allen and Bathurst (2015) developed a formulation that can calculate the load distribution factor and influence factors.

The values of the tensile stresses calculated along the reinforcement length after application of the 20 kPa load are shown in Fig. 9. Tensile stresses were determined using the strain values measured from each strain gauges. Since the calibration test can determine which strain value corresponds to the tensile stress value, the value from each strain gauge reading was converted to tensile stress value (Walters *et al.* 2002). The secant slope of the load-strain curve from a constant-rate of tensile test (Fig. 2) is used to define the reinforcement stiffness. The reinforcement load is estimated from the reinforcement stiffness value and corrected strain.

The maximum tensile stress was identified at the third reinforcement layer, occurring at a distance of 1.2 m from the wall face corresponding to 40% of the wall height. In

general, the results obtained from the measurement devices indicated that the existing stresses in the PS were lower than the design stresses resulting from the deformations following the wall construction after the surcharge load application.

As clearly be seen in Fig. 9, at the second reinforcement layer, the tensile stress value was quite low. Furthermore, the reinforcement in the upper layers functioned more effectively, and was also exposed to higher tensile stress. It was seen that the highest tensile stress (6.3 kN/m) acting on the reinforcement was lower than the utilized reinforcement tensile strength (10 kN/m).

The data provided by five pressure cells was used to predict the lateral earth pressure coefficient (K) and the earth pressure distribution. The K value was measured from the lateral and vertical pressure gauges placed at the level of 220 cm above the wall base. The back calculated active K (ranging from 0.18 to 0.22) was lower than the Coulomb K_a (ranging from 0.26 to 0.31).

By using the proposed theoretical methods (Simplified Stiffness Method and K-Stiffness Method) to determine the reinforcement loads, the maximum tensile stress values occurring at the reinforcement levels were calculated. On Figure 10, there are maximum reinforcement loads at the 2nd, 3rd and 4th reinforcement levels calculated using the elongation values obtained from field strain gage measurements. In addition, the load values determined from the pressure cell measurements at the positions of the pressure cells are also plotted on the graph. These reinforcement loads determined as a result of the field measurements and the reinforcement loads calculated using the formulations of the theoretical methods are given comparatively in Figure 10. The measured reinforcement loads for the top 60% of the wall height were in accordance with the loads of the Simplified Stiffness method, while the theoretical methods significantly overestimate the reinforcement loads, particularly close the wall base. Yang *et al.* (2013) and Yu *et al.* (2016) reported similar trends.

Table 3 Parameters of materials in finite element analyses

	Parameter	Value	Unit
Backfill Material	Material Model	Hardening Soil	-
	Material Behavior	Drained	-
	Unit Weight (γ)	21	kN/m^3
	Tangent Stiffness, E^{ref}_{oed}	32000	kN/m^2
	Secant Stiffness, E^{ref}_{50}	32000	kN/m^2
	Unloading Stiffness, E^{ref}_{oed}	96000	kN/m^2
	Poisson's Ratio (ν)	0.300	-
	Effective Cohesion (c')	1	kN/m^2
	Effective Friction Angle (ϕ')	36	°
	Dilatancy Angle (ψ)	0	°
	Interface Rigidity (R_{inter})	0.67	-
Natural Soil	Material Model	Mohr-Coulomb	-
	Material Behavior	Drained	kN/m^3
	Unit Weight (γ)	18	kN/m^2
	Elastic Modulus (E_{ref})	13000	kN/m^2
	Poisson's Ratio (ν)	0.30	kN/m^2
	Effective Cohesion (c')	1	-
	Effective Friction Angle (ϕ')	31	kN/m^2
	Dilatancy Angle (ψ)	1	°
	Interface Rigidity (R_{inter})	0.67	°
Reinforcement	Material Model	Linear Elastic	-
	Axial Stiffness (EA)	10	kN/m
Facing Elements	Material Model	Linear Elastic	-
	Axial Stiffness (EA)	7250*10^6	kN/m
	Flexural Rigidity (EI)	2500*10^4	kNm^2/m
	Poisson's Ratio (ν)	0.2	-

5. Finite element analyses

5.1 Numerical model

The 3 m-high RSRW constructed in the field was simulated with 2D plane strain analyses using the Plaxis 2D software program (Plaxis 2D 2004). For the FEM model, a system was designed consisting of four basic elements – front facing elements, polymer reinforcement, fill material and natural soil.

5.2 Parameters

The behavior of the natural soil and the drainage material were represented by the Mohr-Coulomb material model, while the behavior of the fill material was represented by the Hardening Soil model. The reinforcements were modelled with flexible geogrid elements. Also, three-node beam elements (plates) with normal stiffness and flexural rigidity were used to model the facing elements. The rest of details for soil and wall facing, the locations of reinforcement layers were the same as in the field model. All of the parameters and their values used in the finite element analysis, consisting of 15-node triangular elements, are presented in Table 3.

There have been many earlier carried out to define the stiffness values of geosynthetic reinforcements considering strain-dependent properties. The technical manual of the polymer strips details the ultimate tensile strength, ultimate strain and the geogrid elements (reinforcements) were modelled accordingly with an axial stiffness (EA). Three pairs of nodes of interface elements were preferred to use for simulating the interactions between the soil, the reinforcement and the facing element. Plaxis 2D was used to model the contact between soil and different materials through interface elements with elastoplastic behavior, which was created by considering friction angle, cohesion and dilatability of the soil (Plaxis 2012).

Among the values in Table 3, unit weight, modulus of elasticity, poison ratio and internal friction angle parameters are the values of the materials used in filed model studies.

Table 4 Maximum tensile stress change on reinforcements (comparison of reinforcement loads)

Reinforcement Layer	Calculated Tensile Stress along Reinforcement Length (kN/m)	Measured Tensile Stress along Reinforcement Length (kN/m)
4	4.57	4.45
3	6.36	6.30
2	2.94	2.90
1	2.25	Not Available

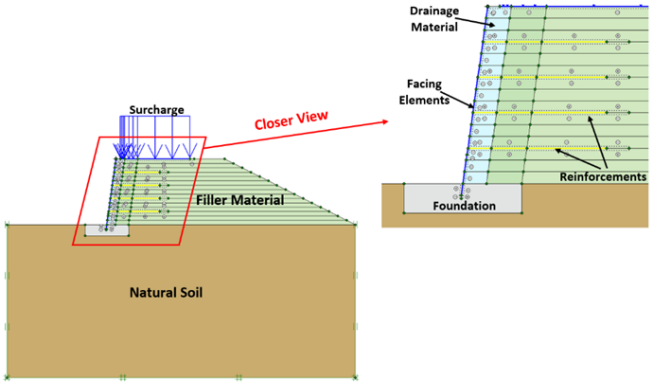

(a) Section view of the system

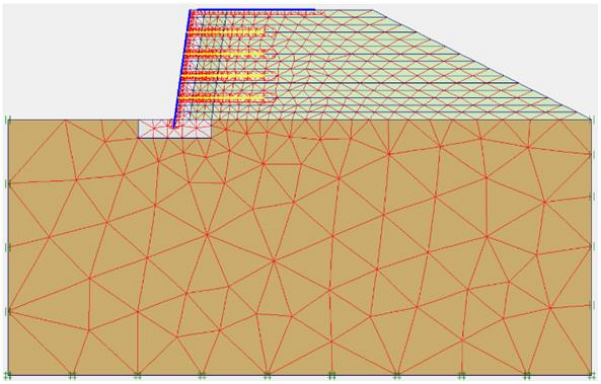

(b) Finite element mesh

Fig. 11 Finite element model

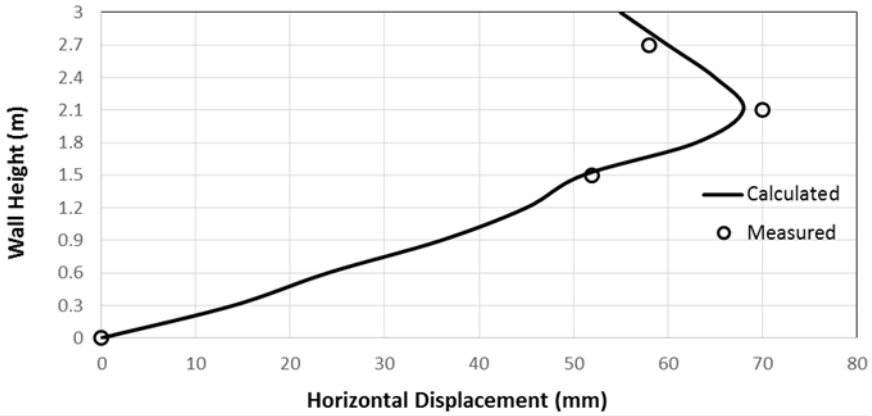

Fig. 12 Measured and calculated horizontal displacements of wall face

These values are determined in the laboratory. Only the R_{inter} value was constantly changed during the calibration of the FEM model results with the field tets values. The R_{inter} value, which provides the necessary verification, is included in the Table 3.

Initially, R_{inter} value of the facing element-filling material were employed to be 0.3 (Damians *et al.* 2015). Considering the work of Damians *et al.* (2015), the R_{inter} value of the reinforcement-fill material was chosen as 0.67 for the first meter of reinforcement length. And for the

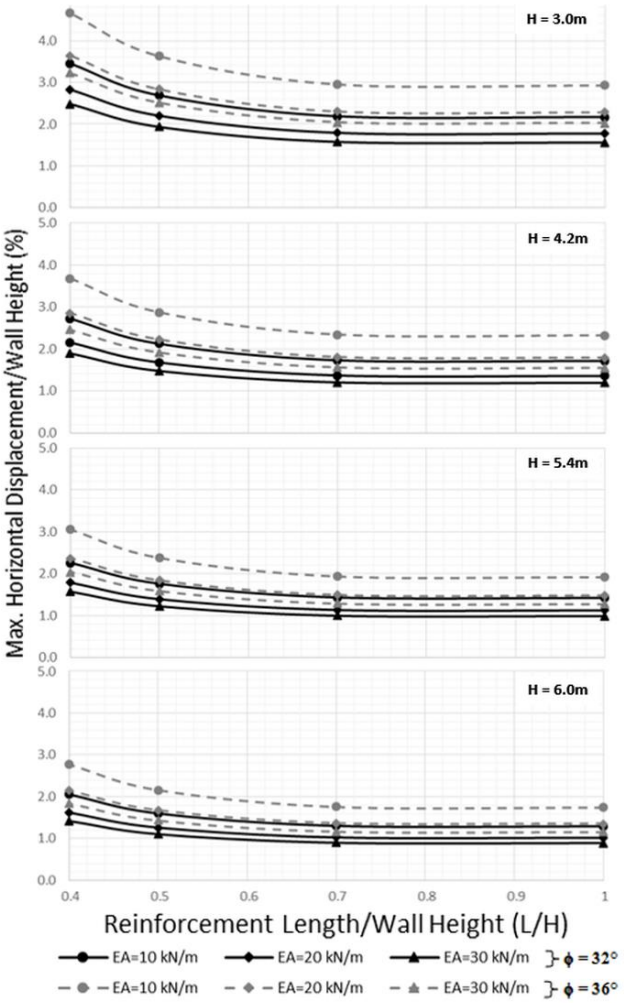

Fig. 13 Parameter effects on horizontal deformation of the wall

remaining length, a value of 1.0 indicating the perfect bond between the reinforcement and the soil was chosen. As mentioned in the work of Yu *et al.* (2015), the length of interface for each reinforcement layer was extended by 0.50m to avoid stresses at the reinforcement end points.

5.3 Verification of the model

A stage construction process was taken into account to attain accurate horizontal displacements. The analysis involved 25 different calculation steps that included the geostatic system state, the excavation of the area where the reinforced earth retaining wall was to be constructed, the spread of each 60 cm-thick fill material in two layers, the placement of the reinforcement and facing elements, the fill material and the 20 kN/m^2 surcharge load application. In the FEM model, the model limits were 50m in both vertical and horizontal direction, being 3 times the height of the wall so as to minimize the boundary effect. A cross section of the constructed FEM model is given in Fig. 11.

The refinement of the finite element mesh, the elasticity modulus of the fill material, the interface stiffness of the fill material–reinforcement and the interface stiffness of the facing element–fill material values were adjusted to concur with the wall horizontal displacement and reinforcement strain values of the FEM model and the measured values throughout the conducted field tests. The results of the analyses, and the tensile stress distributions acting along the length of the reinforcement layers are given in Table 4.

Table 4 presents a comparison of measured and numerical tensile stresses. The numerically predicted tensile loads in the reinforcements indicate in accordance with the measured values at field model and the overall stress distribution is in accordance with other published experimental results as well (Yang *et al.* 2013, Kim and Won 2005).

After the construction stages and the application of the surcharge load, the displacements of the wall and the stresses acting on the reinforcement layers were calculated. At the construction stage, the maximum horizontal wall deformation was approximately 39 cm, and increased to 66 cm when the surcharge load was applied.

After the application of the surcharge loading, the deformation of the potential slip surface was approximately half of the horizontal displacement seen at the top of the wall. After a certain distance, however, no horizontal soil deformation was seen. In Fig. 12, the horizontal displacements values on the wall face are given. The overlap of the measured and calculated values was realized and the validation of the FEM model was completed.

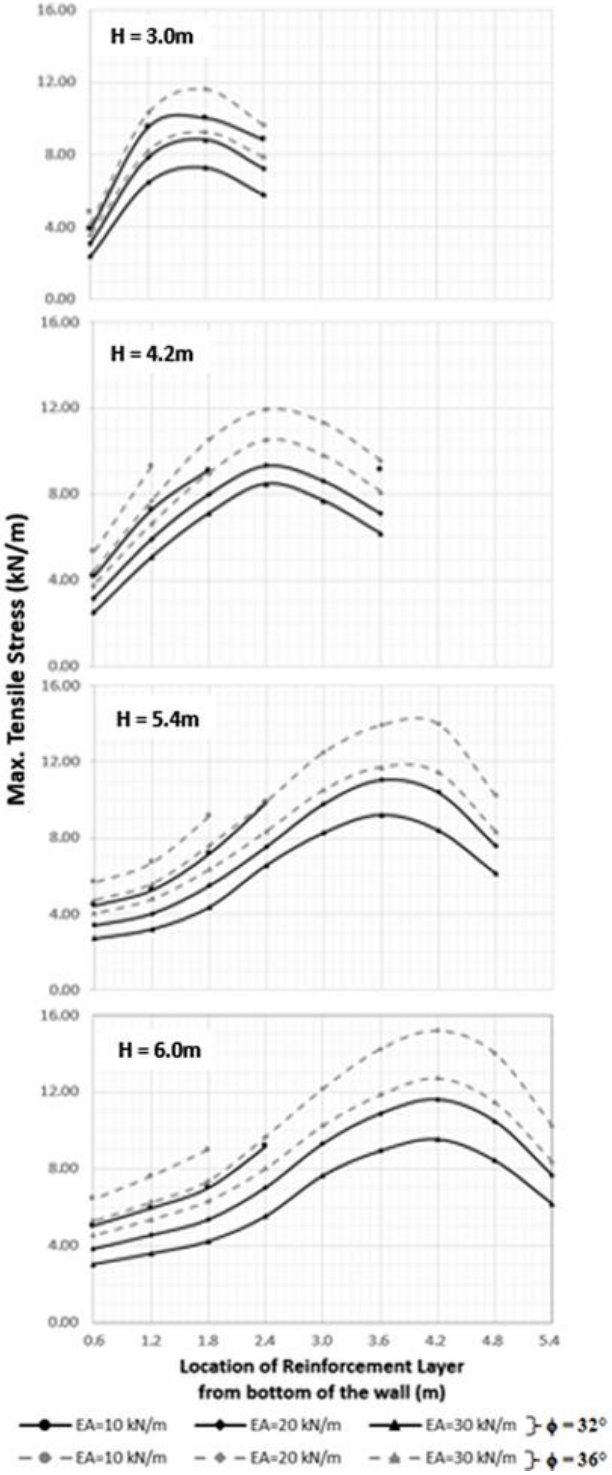

Fig. 14 Parameter effects on tensile stresses of the wall

6. Parametric analyses

Various parametric analyses on validated FEM model were carried out for collapses of RSRW at different heights with different filler material and reinforcement properties. The effects of such parameters as wall height (H), the strength of the reinforcement and fill materials, and reinforcement length (L) on horizontal displacements in the wall were investigated. In this parametric study, comprising 96 finite element analyses, four different wall heights (H), three different reinforcement lengths (L), three different reinforcement strengths (EA) and two different fill materials were used. The parameter properties used in the analyses are presented in Table 5.

36 degrees, which is one of the two internal friction angle terms given in the Table 5, is the in-situ internal friction angle value of compacted fill material used in the field model. The purpose of using this 36 degree value and

Table 5 Parameters used in the numerical analyses

	Values
Wall Height (m)	H = 6.0 m
	H = 5.4 m
	H = 4.2 m
	H = 3.0 m
Reinforcement Length	L = 1.0 H
	L = 0.7 H
	L = 0.5 H
	L = 0.4 H
Fill Material Friction Angle (ϕ')	ϕ'= 32°
	ϕ'= 36°
Reinforcement Tensile Strength (EA)	EA = 10 kN/m
	EA = 20 kN/m
	EA = 30 kN/m

a lower value as 32 degrees in parametric analysis is to see the effects of fill materials that are not properly compacted. The most important reason observed for the failure of earth retaining walls that we have experienced in our country is the fill material that has not been compacted enough.

The effects of the length (L) on horizontal deformation are summarized for four different wall heights (H) in Fig. 13. Based on Fig. 13, as the length of the reinforcement material was increased, the horizontal deformations on the walls decreased, and this effect disappeared at lengths longer than 70% of the wall height. Fig. 13 shows that an increase in L/H ratio from 0.4 to 0.7 caused a 40% reduction in horizontal deformations. When the same reinforcement and fill materials were utilized, increment in wall height increased the horizontal deformations; however, the ratio of the maximum horizontal deformation to wall height was reduced. Also lower horizontal wall deformations will be seen with an increase in the stiffness of fill material.

In addition, it was observed that a decrease in horizontal deformation occurs when the reinforcement length reaches the boundary of the Rankine failure plane. Hence, both the location of the Rankine failure plane and reinforcement length has a significant effect on horizontal deformation (Kibria *et al.* 2014).

The effects of reinforcement stiffness (EA) on horizontal deformation are investigated for four different wall heights and for friction angle of 32° and 36° respectively. The maximum horizontal deformations were decreased in case of the increase in tensile strength of the reinforcement. At the situation that parameters of fill material and reinforcement length no changes, horizontal deformation decreased 35% due to an increase in reinforcement stiffness.

Furthermore, the effects of the strength parameters of the filler and reinforcement materials on the loads acting on the reinforcements are given in Fig. 14 at a standard reinforcement length of 0.7H. As shown in Fig. 14, an increase in stiffness of fill material resulted in lower load values on the reinforcements. The maximum reinforcement loads were found to be on 0.6H from the wall base, at a distance of 0.4H from the face of the wall. An increase in reinforcement stiffness caused a 15% reduction on maximum load on the layer of 0.6H.

7. Conclusions

Within this paper, field model tests that focus on the deformation behavior of PS-RSRW were discussed in detail. The tensile stresses occurred on reinforcements and the wall horizontal displacements were measured. The impact of wall height, stiffness and length of reinforcement, and stiffness fill materials on the behavior of RSRW were investigated with calibrated FEM model. The following conclusions were achieved:

• The estimated horizontal displacements by FEM model resulted in accordance with measured horizontal displacements.

• The maximum horizontal displacement on the front face of the wall was observed at 70% of the wall height from the wall base with a variation of 1.9-3.1% of the wall height.

• The maximum reinforcement loads, were found to be on 60% of the wall height from the wall base, occurred at a distance of 40% of the wall height from the face of the wall.

• The measured and the numerically predicted active lateral earth pressure coefficient was lower than the Coulomb active lateral earth pressure coefficient. The theoretical methods significantly overestimate the tensile loads, especially close the wall base.

• When the same reinforcement and fill materials were utilized, increment in wall height increased the horizontal deformations; however, the ratio of the maximum horizontal deformation to wall height was reduced.

• The maximum horizontal deformations were decreased in the case of an increase in tensile strength of the reinforcement.

Acknowledgments

The study was supported with funding from Muğla Sıtkı Koçman University Scientific Research Project Coordinatorship with Project Code: 14-057. The financial support from the Coordinatorship is gratefully acknowledged. The authors would like to thank East Inşaat ve Dış Ticaret Corp., which provided project management and civil engineering services for polymer strip reinforced soil walls at the site.

References

AASHTO (2002), *Standard Specifications for Highway Bridges*, 17th Edition, American Association of State Highway and Transportation Officials, Washington, D.C., U.S.A.

Abdelouhab, A., Dias, D. and Freitag, N. (2011), "Numerical analysis of the behavior of mechanically stabilized earth walls reinforced with different types of strips", *Geotext. Geomembranes*, **29**(2), 116-129. https://doi.org/10.1016/j.geotexmem.2010.10.011.

Allen, T.M. and Bathurst, R.J. (2002), "Soil reinforcement loads in

geosynthetic walls at working stress conditions", *Geosynth. Int.*, **9**(11), 525-566. https://doi.org/10.1680/gein.9.0227.

Allen, T.M. and Bathurst, R.J. (2014), "Design and performance of 6.3-m-high, block-faced geogrid wall designed using K-stiffness method", *J. Geotech. Geoenviron. Eng.*, **140**(2), 04013016. https://doi.org/10.1061/(ASCE)GT.1943-5606.0001013.

Allen, T.M. and Bathurst, R.J. (2015), "Improved simplified method for prediction of loads in reinforced soil walls", *J. Geotech. Geoenviron. Eng.*, **141**(11), 04015049. https://doi.org/10.1061/(ASCE)GT.1943-5606.0001355.

Allen, T.M. and Bathurst, R.J. (2018), "Application of the simplified stiffness method to design of reinforced soil walls", *J. Geotech. Geoenviron. Eng.*, **144**(5), 04018024. https://doi.org/10.1061/(ASCE)GT.1943-5606.0001874.

Altunbas, A., Soltanbeigi, B. and Cinicioglu, O. (2017), "Determination of active failure surface geometry for cohesionless backfills", *Geomech. Eng.*, **12**(6), 983-1001. https://doi.org/10.12989/gae.2017.12.6.983.

Balaban, E. and Onur, M.İ. (2018), "Comparison of behavior of basal reinforced piled embankment with two layer of reinforcement", *Geomech. Eng.*, **16**(3), 233-245. https://doi.org/10.12989/gae.2018.16.3.233

Bathurst, R.J., Miyata, Y., Nernheim, A. and Allen, T.M. (2008), "Refinement of K-stiffness method for geosynthetic reinforced soil walls", *Geosynth. Int.*, **15**(4), 269-295. https://doi.org/10.1680/gein.2008.15.4.269.

Bathurst, R.J., Nernheim, A., Walters, D.L, Allen, T.M., Burgess, P. and Saunders, D.D. (2009), "Influence of reinforcement stiffness and compaction on the performance of four geosynthetic-reinforced soil walls", *Geosynth. Int.*, **16**(1), 43-59. https://doi.org/10.1680/gein.2009.16.1.43.

Bathurst, R.J., Walters, D., Vlachopoulos, N., Burgess, P. and Allen, T.M. (2000), "Full scale testing of geosynthetic reinforced walls", *Proceedings of Geo-Denver*, Denver, Colorado, U.S.A., August.

Bilgin, O. and Mansour, E. (2014), "Effect of reinforcement type on the design reinforcement length of mechanically stabilized earth walls", *Eng. Struct.*, **59**, 663-673. https://doi.org/10.1016/j.engstruct.2013.11.013.

Bourgeois, E., Soyez, L. and Le Kouby, A. (2011), "Experimental and numerical study of the behavior of a reinforced-earth wall", *Comput. Geotech.*, **38**, 515-525. https://doi.org/10.1016/j.compgeo.2011.02.017.

Castorina, S.V., Lopes, M.L. and Caldeira, L. (2015), "Sand-Nonwoven geotextile interfaces shear strength by direct shear and simple shear tests", *Geomech. Eng.*, **9**(5), 601-618. https://doi.org/10.12989/gae.2015.9.5.601.

Christopher, B., Gill, S., Giroud, J.P., Juran, I., Schlosser, F., Mitchell, J.K. and Dunnicliff, J. (1990), *Reinforced Soil Structure-Design and Construction Guideline*, Federal Highway Administration, Washington, D.C., U.S.A.

Collin, J. (1997), *Design Manual for Segmental Retaining Walls*, (2nd Edition), National Concrete Masonry Association (NCMA), Virginia, U.S.A.

Cristelo, N., Félix, C., Lopes, M.L. and Dias, M. (2016), "Monitoring and numerical modelling of an instrumented mechanically stabilised earth wall", *Geosynth. Int.*, **23**(1), 48-61. https://doi.org/10.1680/jgein.15.00032.

Damians, I.P., Bathurst, R.J., Josa, A. and Lloret, A. (2015), "Numerical analysis of an instrumented steel-reinforced soil wall", *Int. J. Geomech.*, **15**(1), 1-15. https://doi.org/10.1061/(ASCE)GM.1943-5622.0000394.

Ehrlich, M. and Mirmoradi, S.H. (2013), "Evaluation of the effects of facing stiffness and toe resistance on the behavior of GRS walls", *Geotext. Geomembranes,* **40**, 28-36. https://doi.org/10.1016/j.geotexmem.2013.07.012

Elias, V., Christopher, B.R. and Berg, R.R. (2001), *Mechanically Stabilized Earth Walls and Reinforced Soil Slopes-Design and Construction Guidelines*, Federal Highway Administration, Washington, D.C., U.S.A.

Elias, V. and Christopher, B.R. (1996), *Mechanically Stabilized Earth Walls and Reinforced Soil Slopes-Design and Construction Guidelines*, Federal Highway Administration, Washington, D.C., U.S.A.

Fattah, M.Y., Yousif, M.A. and Salim, H.D. (2009), "Finite element analysis of reinforced earth walls", *J. Eng. Sustain. Develop.*, **13**(3), 87-108.

Güler, E. (2006), "Geosentetik donatili istinat duvari bir şartname taslaği", *İkinci Ulusal Geosentetikler Konferansı*, Istanbul, Türkiye, November.

Hatami, K. and Bathurst, R.J. (2005), "Development and verification of a numerical model for the analysis of geosynthetic-reinforced soil segmental walls under working stress conditions", *Can. Geotech. J.*, **42**(4), 1066-1085. https://doi.org/10.1139/t05-040.

Horpibulsuk, S., Suksiripattanapong, C., Niramitkornburee, A., Chinkulkijniwat, A. and Tangsutthinon, T. (2011), "Performance of an earth wall stabilized with bearing reinforcements", *Geotext. Geomembranes*, **29**(5), 514-524. https://doi.org/10.1016/j.geotexmem.2011.05.002.

Holtz, R.D., Christopher, B.R. and Berg, R.R. (1997), *Geosynthethic Engineering*, Bi-Tech Publishers Ltd, Richmond, British Columbia, Canada.

Holtz, R.D. and Lee, W.F. (2002), "Internal stability analyses of geosynthetic reinforced retaining walls", Research Report Agreement No. T9903, Task 95 Geosynthetic Reinforcement III; Washington State Transportation Commission Department of Transportation and in cooperation with U.S. Department of Transportation Federal Highway Administration, Washington, U.S.A.

Huang, B., Bathurst, R.J. and Hatami, K. (2009), "Numerical study of reinforced soil segmental walls using three different constitutive soil models", *J. Geotech. Geoenviron. Eng.*, **135**(10), 1486-1497. https://doi.org/10.1061/(ASCE)GT.1943-5606.0000092.

Jones, C.J.F.P. (1996), *Earth Reinforcement and Soil Structures*, Thomas Telford Ltd., London, U.K.

Kaya, T. (2007), "Behavior of reinforced earth structures under earthquakes", M.Sc. Thesis, Boğaziçi University, Istanbul, Turkey.

Kayadelen, C., Önal, T.Ö. and Altay, G. (2018), "Experimental study on pull-out response of geogrid embedded in sand", *Measurement*, **117**, 390-396. https://doi.org/10.1016/j.measurement.2017.12.024.

Kibria, G., Hossain, S. and Khan M.S. (2014), "Influence of soil reinforcement on horizontal displacement of MSE wall", *Int. J. Geomech.*, **14**(1), 5-8. https://doi.org/10.1061/(ASCE)GM.1943- 5622.0000297.

Kim, S. and Won, M.S. (2005), "Deformation behaviors and finite element analyses of geosynthetic reinforced soil walls", *KSCE J. Civ. Eng.*, **9**(5), 363-369. https://doi.org/10.1007/BF02830627.

Kongkitkul, W., Tatsuoka, F., Kawahata, S., Hirakawa, D., Sugimoto, T. and Ito, M. (2010), "Time histories of tensile force in geogrid arranged in two full-scale high walls", *Geosynth. Int.*, **17**(1), 12-32. https://doi.org/10.1680/gein.2010.17.1.12.

Lee, K.L, Adams, B.D. and Vaneron J.J. (1973), "Reinforced earth retaining walls", *J. Soil Mech. Found Div.*, **99**(10), 745-764. https://doi.org/10.1061/JSFEAQ.0001931.

Liu, H., Yang, G., Wang, H. and Xiong, B. (2017), "A large-scale test of reinforced soil railway embankment with soil bag facing under dynamic loading", *Geomech. Eng.*, **12**(4), 579-593. https://doi.org/10.12989/gae.2017.12.4.579

Leshchinsky, D. and Han, J. (2004), "Geosynthetic reinforced

multitiered walls", *J. Geotech. Geoenviron. Eng.*, **130**(12), 1225. https://doi.org/10.1061/(ASCE)1090-0241(2004)130:12(1225).

Mahmood, T. (2009), "Failure analysis of a mechanically stabilized earth (MSE) wall using finite element program Plaxis", M.Sc. Thesis, Arlington Texas University, Arlington, U.S.A.

Mendonça A., Lopes, M. and Pinho-Lopes, M. (2003), "Construction and post-construction behaviour of a geogrid-reinforced steep slope", *Geotech. Geol. Eng.*, **21**(2), 129-147. https://doi.org/10.1023/A:1023504415859.

Ouria, A., Toufigh, V., Desai, C., Toufigh, V. and Saadatmanesh, H. (2016), "Finite element analysis of a CFRP reinforced retaining wall", *Geomech. Eng.*, **10**(6), 757-774. https://doi.org/10.12989/gae.2016.10.6.757.

Plaxis (2012), *Material Models Manual*, Delft University of Technology, Delft, The Netherlands.

Plaxis 2D (2004), Plaxis finite element code for soil and rock analysis manual, Delft University of Technology and Plaxis, Delft, The Netherlands.

Perkins, S.W. and Lapeyre, J.A. (1997), "In-isolation strain measurement of geosynthetics in wide-width strip tension test", *Geosynth. Int.*, **4**(1),11-32. https://doi.org/10.1680/gein.4.0086.

Riccio, M., Ehrlich, M. and Dias, D. (2014), "Field monitoring and analyses of the response of a block-faced geogrid wall using fine grained tropical soils", *Geotext. Geomembranes*, **42**(2), 127-138. https://doi.org/10.1016/j.geotexmem.2014.01.006.

Salem, M.A., Hammad, M.A. and Amer, M.I. (2018), "Field monitoring and numerical modeling of 4.4 m-high mechanically stabilized earth wall", *Geosynth. Int.*, **25**(5), 545-559. https://doi.org/10.1680/jgein.18.00027.

Sawicki, A. (2000), *Mechanics of Reinforced Soil*, CRC Press, Brookfield, Vermont, U.S.A.

Seed, H.B. and Whitman, R.V. (1970), "Design of earth retaining structures for dynamic loads", *Proceedings of the Speciality Conference on Lateral Stresses and Earth Retaining Structures,* Ithaca, New York, U.S.A., June.

Segrestin, P. and Bastick, M.J. (1988), "Seismic design of reinforced earth retaining walls: the contribution of finite element analysis", *Proceedings of the International Symposium on Theory and Practice of Earth Reinforcement*, Kyushu, Japan, October.

Song, F. and Tian, Y. (2019), "Three-dimensional numerical modelling of geocell reinforced soils and its practical application", *Geomech. Eng.*, **17**(1), 1-9. https://doi.org/10.12989/gae.2019.17.1.001.

Vidal, H. (1969), "The principal of reinforced earth", *Highway Eng. Rec.*, **282**, 1-16.

Vieira, C.S., Lopes, M.D.L. and Caldeira, L.M. (2011), "Earth pressure coefficients for design of geosynthetic reinforced soil structures", *Geotex. Geomembranes*, **29**(5), 491-501. https://doi.org/10.1016/j.geotexmem.2011.04.003.

Walters, D.L., Allen, T.M., and Bathurst, R.J. (2002), "Conversion of geosynthetic strain to load using reinforcement stiffness", *Geosynth. Int.*, **9**(5-6), 483-523. https://doi.org/10.1680/gein.9.0226.

Won, M.S. and Kim, Y.S (2006), "Application of strain gauges to measure nonwoven geotextile deformation in reinforced soil wall. In J. Kuwano and J. Koseki (Eds.)", *Proceedings of the 8th International Conference on Geosynthetics*, Yokohama, Japan, September.

Whitcomb, W. and Bell, J.R. (1979), "Analysis techniques for low reinforced soil retaining walls and comparison of strip and sheet reinforcements", *Proceedings of the 17th Engineering Geology and Soil Engineering Symposium*, Moscow, Russia, April.

Yang, G., Liu, H., Liu, P. and Zhang, B. (2012), "Geogrid-reinforced lime-treated cohesive soil retaining wall: Case study and implications", *Geotext. Geomembranes*, **35**, 112-118. https://doi.org/10.1016/j.geotexmem.2012.09.001.

Yang, G., Liu, H., Liu, Zhou, Y.T. and Xiong, B.L. (2014), "Post-construction performance of a two-tiered geogrid reinforced soil wall backfilled with soil-rock mixture", *Geotext. Geomembranes*, **42**(2), 91-97. http://doi.org/10.1016/j.geotexmem.2014.01.007.

Yang, K.H., Utomo, P. and Liu, T.L. (2013), "Evaluation of force-equilibrium and deformation-based design approaches for predicting reinforcement loads within geosynthetic reinforced soil structures", *J. GeoEng.*, **8**(2), 41-54. https://doi.org/10.6310/jog.2013.8(2).2.

Yu, Y., Bathurst, R.J. and Miyata, Y. (2015), "Numerical analysis of a mechanically stabilized earth wall reinforced with steel strips", *Soils Foundati*, **55**(3), 536-547.
https://doi.org/10.1016/j.sandf.2015.04.006.

Yu, Y., Bathurst, R.J. and Allen, T.M. (2016), "Numerical modelling of the SR-18 geogrid reinforced modular block retaining walls", *J. Geotech. Geoenviron. Eng.*, **142**(5), 04016003. https://doi.org/10.1061/(ASCE)GT.1943-5606.0001438.

IC